Control Engineering Practice 169 (2026) 106769

Contents lists available at ScienceDirect

Control Engineering Practice

journal homepage: www.elsevier.com/locate/conengprac

Kinematic guidance using virtual reference point for underactuated marine vehicles with sideslip compensation

S. K. Mallipeddi [a,*], M. Menghini [a], S. Simani [b], P. Castaldi [a]

[a] Department of Electrical, Electronic and Information Engineering (DEI) "Guglielmo Marconi", University of Bologna, Viale Risorgimento 2, Bologna, 40136, Italy
[b] Department of engineering, University of Ferrara, Via Savonarola, 9, Ferrara, 44121, Italy

A R T I C L E I N F O

Keywords:
Underactuated marine vehicles
Line of sight
Virtual reference point
Guidance
Model predictive control (MPC)

A B S T R A C T

Path following for underwater vehicles remains a significant challenge due to underactuation in the sway and heave directions. Most existing approaches rely on line-of-sight guidance to address this issue. In this paper, we explore an alternative approach using kinematic guidance, based on virtual reference point guidance, wherein a fictitious point offset from the vehicle's center of rotation is used to reformulate the kinematic control problem and mitigate underactuation constraints. While this concept has been explored to some extent, previous works have largely overlooked the impact of the vehicle's attitude. To address this limitation, we propose a solution that simultaneously accounts for the vehicle's attitude while minimizing cross-track error by defining the error dynamics in the body reference frame, which enables direct control of yaw and sway through yaw rate actuation. A model predictive controller is designed to optimize both attitude stabilization and trajectory tracking performance and is enhanced with an adaptive extended Kalman filter-like observer to estimate the sideslip caused by sea currents and external disturbances. The proposed controller is evaluated under the influence of sea currents and modeling uncertainties, and compared to an existing method from the literature, demonstrating its effectiveness in maintaining path-following accuracy while stabilizing the attitude in the presences of the sea currents.

1. Introduction

Autonomous Marine Vehicles (AMVs) are increasingly vital as they allow for long-duration, high-risk, or repetitive tasks to be conducted without direct human presence, significantly reducing costs and increasing safety. AMVs include Autonomous Surface Vehicles (ASVs) and Autonomous Underwater Vehicles (AUVs) that perform various missions including oceanographic surveys (Whitt et al., 2020), environmental monitoring (Di Ciaccio & Troisi, 2021), infrastructure inspection (Nauert & Kampmann, 2023), search and rescue (Mansor et al., 2021), and military operations (Boretti, 2024). Their autonomy enables exploration of hazardous or remote regions, such as deep-sea environments or areas affected by severe weather, that would otherwise be inaccessible. A common characteristic of many AMVs, especially those designed for practical and energy-efficient operations, is that they are underactuated, meaning they possess fewer control inputs than degrees of freedom that need to be controlled. This design choice often simplifies construction, reduces energy consumption, and improves endurance, but it also introduces substantial challenges for precise maneuvering and control (Bhat & Stenius, 2018).

This article focuses on a class of underactuated marine vehicles that operate primarily in the horizontal plane, such as ASVs and AUVs, which maintain depth through dedicated depth controllers (Do & Pan, 2009), with minimal pitching or vertical motion affecting their horizontal dynamics. The primary challenge for these vehicles lies in the path-following problem, where the objective is to ensure that the vehicle converges to and follows a predefined spatial path, independent of the time along that path (Lapierre & Soetanto, 2007). This capability is essential for a wide range of missions, including systematic seabed mapping, pipeline or cable inspection, and environmental sampling, where spatial coverage and precision are critical. Path-following is particularly challenging for underactuated vehicles due to their limited control authority and the influence of external disturbances such as sea currents (Belleter et al., 2019).

To address the path-following problem in underactuated marine vehicles, various guidance laws have been proposed to generate desired

* Corresponding author.
E-mail addresses: sivakumar.mallipedd2@unibo.it (S.K. Mallipeddi), massimilian.menghin3@unibo.it (M. Menghini), silvio.simani@unife.it (S. Simani), paolo.castaldi@unibo.it (P. Castaldi).
URL: https://www.unibo.it/sitoweb/massimilian.menghin3/en (M. Menghini), https://www.unibo.it/sitoweb/paolo.castaldi/en (P. Castaldi)

https://doi.org/10.1016/j.conengprac.2026.106769
Received 28 May 2025; Received in revised form 5 January 2026; Accepted 5 January 2026

headings that steer the vehicle along a predefined path. Among the most widely used are Line-of-Sight (LOS)-based methods (Breivik & Fossen, 2005; Fossen et al., 2003), which compute a desired heading that minimizes the cross-track error, typically using a scalar variable that parametrizes the path. These guidance commands result in yaw rotations that indirectly induce sway motion, thereby compensating for the lack of direct lateral actuation in underactuated systems. The Proportional LOS (PLOS) method introduces a look-ahead distance to improve stability, with a formulation allowing for uniform global stability proposed in Fossen and Pettersen (2014). Time-varying look-ahead distance strategies have also been developed to achieve better transient performance and compensate for external disturbances (Lekkas & Fossen, 2012; Pavlov et al., 2009).

However, PLOS may still exhibit steady-state errors under persistent disturbances such as constant sea currents. To address this limitation, the Integral LOS (ILOS) method (Caharija et al., 2016; Zhang et al., 2024) incorporates an integral term of the cross-track error into the guidance law. This integral action allows the system to reject constant biases and ensures zero steady-state cross-track error (Nie & Lin, 2019). In more advanced scenarios, Adaptive LOS (ALOS) strategies (Fossen & Aguiar, 2024; Kim et al., 2007) integrate real-time estimates of sideslip angles are used in the guidance computation. These methods have been shown to achieve uniform semi-global stability (Fossen & Aguiar, 2024). However, the performance of ALOS depends on the tuning of the adaptation gain: while higher gains can improve convergence speed, they may also lead to undesirable oscillations during transient phases. To mitigate such issues, Extended State Observer-based LOS (ELOS) methods have been proposed (Liu et al., 2016). ELOS leverages an observer framework to estimate both unmeasured states and disturbances, feeding this information back into the guidance system for real-time compensation. Compared to ILOS and ALOS, ELOS offers a more systematic and robust approach to disturbance rejection, particularly when facing complex or time-varying environmental conditions.

Beyond LOS-based approaches, vector field guidance strategies have gained attention for their ability to construct smooth vector fields that guide the vehicle toward the path using gradient-like behaviors (Xu et al., 2020). A comparison between vector field and LOS guidance methods is presented in Caharija et al. (2015). For a comprehensive review of recent advances in LOS guidance strategies, readers are referred to Gu et al. (2022).

While most existing path-following approaches define the control objective relative to the vehicle's pivot point (center of rotation), an alternative concept found in the literature is the use of a Virtual Reference Point (VRP). The VRP is usually placed at the bow of the vehicle, ahead of the pivot point, and offers both theoretical and practical advantages. As demonstrated in Alonge et al. (2001), Berge et al. (1998), selecting a forward-positioned VRP can have a naturally stabilizing effect on the guidance dynamics. This idea is analogous to the intuitive observation that pulling a trolley leads to more stable behavior than pushing it, as discussed in Degorre et al. (2024a). Beyond its stabilizing role, the VRP framework is advantageous in applications requiring sensor-driven navigation. For example, in seabed scanning or inspection tasks, sensors such as cameras or sonar are typically mounted at a location offset from the vehicle's center of rotation. By choosing the VRP to coincide with the sensor location, as suggested in Matouš et al. (2024), the guidance law can directly regulate the path of the sensor itself, enabling more accurate coverage and improving mission performance.

Another significant advantage of the VRP lies in its ability to help address the underactuation problem by leveraging the kinematic coupling introduced by the displacement between the VRP and the vehicle's pivot point. As illustrated conceptually in Paliotta et al. (2018), let P denote the pivot point, and P_v denote the virtual reference point located a distance E ahead as shown in Fig. 1. A surge force applied at P results in a corresponding motion at P_v in the surge direction. Similarly, applying a yaw torque around point P induces a sway component at P_v due to the offset E. This coupling effect allows sway-like actuation to emerge from the available inputs–despite the vehicle being underactuated. This concept has been further explored in Degorre et al. (2024b), where a control-oriented "handy matrix" formulation is proposed to map available actuation to the dynamics at the VRP, effectively exploiting this coupling to overcome underactuation. However, this mapping may yield multiple solutions, not all of which are physically meaningful or robust for control, as discussed in Matouš et al. (2025). Moreover, using the VRP enables the vehicle's kinematics to be modeled similarly to nonholonomic systems, thus allowing the application of a wide range of nonlinear control strategies developed for such systems. For example, output feedback linearization can be employed by selecting the VRP as the output point, as demonstrated in Matouš et al. (2024, 2025), Paliotta et al. (2018). This modeling approach not only enhances controllability but also integrates naturally with perception-driven navigation tasks.

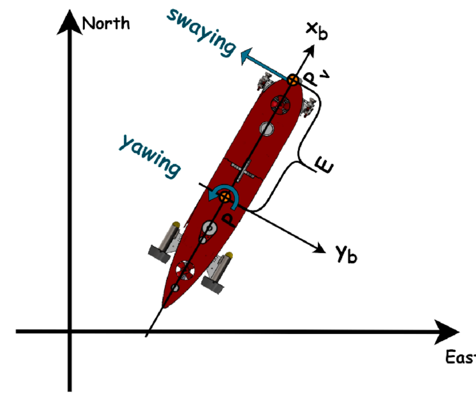

Fig. 1. Schematic representation of the VRP located ahead of the pivot point by a distance E, introducing kinematic coupling between yaw and sway motions in underactuated marine vehicles.

To the best of the authors' knowledge, existing literature on guidance of underactuated AMVs using VRP guidance has primarily focused on the path-following problem, without explicitly addressing attitude tracking. In works such as Degorre et al. (2024a,b), the vehicle's attitude is assumed to remain stable due to the internal dynamics, but it is not regulated to follow a desired orientation. Similarly, in the output feedback linearization frameworks proposed in Degorre et al. (2025), Matouš et al. (2024, 2025), Paliotta et al. (2018), the attitude dynamics are treated as internal and proven to be bounded, but not necessarily tracking a reference. In this work, we aim to bridge this gap by introducing a Nonlinear Model Predictive Control (NMPC) strategy that explicitly addresses both path-following and attitude regulation. The motivation for using an NMPC framework stems from the inherent kinematic coupling induced by the VRP, where sway and yaw motions are interdependent and influenced by a common set of control inputs. While previous approaches focused primarily on sway control and treated yaw behavior as a secondary or bounded effect, the proposed controller jointly optimizes both sway and yaw dynamics to achieve coordinated motion. Furthermore, we develop an Adaptive Extended Kalman Filter (AEKF)-based observer to estimate the unknown sideslip angle, which is critical for accurate attitude tracking and compensation under environmental disturbances, such as sea currents.

The remainder of this paper is organized as follows. Section 2 presents the dynamic model of the AMVs considered in this study. Section 3 formulates the path-following problem using the VRP framework. Section 4 describes the design of the AEKF observer used to estimate the sideslip angle. Section 5 details the two-loop control strategy–comprising the guidance and control loops–with a primary focus on the NMPC. Section 6 provides simulation results demonstrating the effectiveness of the proposed method under sea current conditions, using the a AUV called "Blucy" as a case study. Finally, Section 7 concludes the paper and outlines directions for future work.

2. Vehicle model

In this study, we consider a planar three-degree-of-freedom (3-DOF) model (Fossen, 2011), suitable for a class of AUVs and ASVs that predominantly move in the horizontal plane. Vertical dynamics are excluded from this model under the assumption that they are either negligible or managed independently by a separate depth control system.

The vehicle's motion is defined in the North-East-Down (NED) inertial frame $\langle I \rangle$, where the position and orientation vector is given by $\eta = [x, y, \psi]^T \in \mathbb{R}^3$. The body-fixed velocity vector is $\nu = [u, v, r]^T \in \mathbb{R}^3$, representing surge, sway, and yaw rate, respectively. The rotation matrix that transforms velocities from the body frame $\langle b \rangle$ to the inertial frame is defined as:

$$J(\psi) = \begin{bmatrix} \cos\psi & -\sin\psi & 0 \\ \sin\psi & \cos\psi & 0 \\ 0 & 0 & 1 \end{bmatrix}, \quad J(\psi) \in SO(2) \tag{1}$$

where $SO(2)$ denotes the special orthogonal group of planar rotations.

The vehicle dynamics are described by the standard marine model as follows:

$$\dot{\eta} = J(\psi)\nu \tag{2a}$$

$$M\dot{\nu} + C(\nu)\nu + D(\nu)\nu = \tau_p + d(t) \tag{2b}$$

where $M \in \mathbb{R}^{3\times3}$ is the total inertia matrix composed of rigid-body inertia and added mass; $C(\nu) \in \mathbb{R}^{3\times3}$ is the Coriolis-centripetal matrix including added mass effects; $D(\nu) \in \mathbb{R}^{3\times3}$ is the hydrodynamic damping matrix, incorporating both linear and nonlinear terms; $\tau_p = [\tau_u, 0, \tau_r]^T \in \mathbb{R}^3$ is the control input vector; and $d(t) = [d_u, d_v, d_r]^T \in \mathbb{R}^3$ represents unknown environmental disturbances such as sea currents and unmodeled dynamics. The absence of a control input in the sway direction reflects an underactuated configuration common in many marine vehicles.

To facilitate control design, we adopt the following assumptions:

Assumption 1. The vehicle exhibits port-starboard symmetry, i.e., its dynamics are invariant under reflection about its longitudinal axis.

Remark 1. This symmetry is typical of marine vehicles with streamlined hulls. It allows the neglect of certain off-diagonal terms in the added mass and damping matrices, simplifying the dynamic equations (Fossen, 2011).

Assumption 2. Hydrodynamic damping is considered to be linear with respective to the velocity of the Vehicle.

Remark 2. Linear hydrodynamic damping is reasonable in low-speed operating conditions where nonlinear effects are minimal. Furthermore, the nonlinear damping terms, while neglected in this model, generally have a stabilizing effect, as they introduce energy dissipation that naturally enhances system stability.

Assumption 3. The external disturbances $d(t)$ are bounded such that $|d_n| \le \bar{d}_n$ for $n = u, v, r$, where $\bar{d}_n$ are unknown but finite constants.

Remark 3. This models real-world effects like current, wind, or wave-induced forces that, although uncertain, are naturally constrained by environmental limits.

Under Assumptions 1-3, and by resolving the vector-matrix equations into scalar components, the vehicle model can be reformulated as:

$$\dot{x} = u\cos\psi - v\sin\psi \tag{3a}$$

$$\dot{y} = u\sin\psi + v\cos\psi \tag{3b}$$

$$\dot{\psi} = r \tag{3c}$$

$$\dot{u} = F_u(u, v, r) + \tau_u + d_u \tag{4a}$$

$$\dot{v} = Y(u)v + X(u)r + d_v \tag{4b}$$

$$\dot{r} = F_r(u, v, r) + \tau_r + d_r \tag{4c}$$

where the functions F_u, F_r, $X(u)$, and $Y(u)$ are defined as:

$$\begin{aligned} F_u(u, v, r) &= \frac{1}{m_{11}}(m_{22}v + m_{23}r)r - \frac{d_{11}}{m_{11}}u \\ F_r(u, v, r) &= \frac{m_{23}d_{22} - m_{22}(d_{32} + (m_{22} - m_{11})u)}{m_{22}m_{33} - m_{23}^2}v \\ &\quad + \frac{m_{23}(d_{23} + m_{11}u) - m_{22}(d_{33} + m_{23}u)}{m_{22}m_{33} - m_{23}^2} \\ X_1 &= \frac{m_{11}m_{33} - m_{23}^2}{m_{22}m_{33} - m_{23}^2}, \quad X_2 = \frac{d_{33}m_{23} - d_{23}m_{33}}{m_{22}m_{33} - m_{23}^2} \\ Y_1 &= \frac{(m_{11} - m_{22})m_{23}}{m_{22}m_{33} - m_{23}^2}, \quad Y_2 = \frac{d_{22}m_{33} - d_{32}m_{23}}{m_{22}m_{33} - m_{23}^2} \\ X(u) &= -X_1u + X_2, \quad Y(u) = -Y_1u - Y_2 \end{aligned} \tag{5}$$

Here, m_{ij} and d_{ij} denote the entries of the inertia matrix M and the damping matrix D.

3. Problem formulation

Let $P = [x, y]^T \in \mathbb{R}^2$ denote the position of the pivoting point expressed in the inertial frame $\langle I \rangle$. Traditionally, this point is used for path-following problems. In this study, the VRP, denoted by $P_v \in \mathbb{R}^2$, is used for path following. The relation between P and P_v is given by:

$$P_v = P + R(\psi)E \tag{6}$$

where $E = [E_x, E_y, E_z]^T \in \mathbb{R}^2$ represents the position vector from the pivoting point P to the virtual point P_v in body frame $\langle b \rangle$. It is chosen such that $E_x > 0$ and $E_y = 0$, placing the VRP at the bow of the vehicle. The matrix $R(\psi) \in SO(2)$ represents the rotation matrix from body to inertial frame and is expressed as:

$$R(\psi) = R = \begin{bmatrix} \cos\psi & -\sin\psi \\ \sin\psi & \cos\psi \end{bmatrix} \tag{7}$$

Consider a reference path $\mathcal{P}$ parameterized as $P_d = \left[x_d(\varsigma), y_d(\varsigma)\right]^T \in \mathbb{R}^2$, with a scalar path variable $\varsigma \in \mathbb{R}$ that moves along the path with velocity $U_d > 0$.

Assumption 4. The reference path $\mathcal{P}$ is smooth and at least twice differentiable (C^2) to ensure well-defined curvature and tangent vectors.

Let the frame $\langle P \rangle$, referred to as the local path-tangent frame, is defined such that its x-axis is aligned with the tangent to the path at $P_d(\varsigma)$ and its y-axis is normal to the path. This frame moves along the path with velocity U_d, and the variable ς is updated according to:

$$\dot{\varsigma} = \frac{U_d}{\sqrt{{x'_d}^2(\varsigma) + {y'_d}^2(\varsigma)}} \tag{8}$$

This ensures that the frame $\langle P \rangle$ continuously tracks the motion along the path, providing a convenient moving reference. The angle between this frame and inertial frame $\langle I \rangle$ is denoted by γ_d, and it is computed as:

$$\gamma_d = \text{atan2}\left(y'(\varsigma), x'(\varsigma)\right) \tag{9}$$

where $x'(\varsigma) = \frac{dx_d}{d\varsigma}$ and $y'(\varsigma) = \frac{dy_d}{d\varsigma}$. The associated rotation matrix $R_p(\gamma_d) \in SO(2)$ is given by:

$$R_p(\gamma_d) = R_p = \begin{bmatrix} \cos\gamma_d & -\sin\gamma_d \\ \sin\gamma_d & \cos\gamma_d \end{bmatrix} \tag{10}$$

The path-following error between the vehicle's VRP and the desired path, expressed in the body frame, is defined as:

$$\varepsilon = R(\psi)^T(P_d - P_v) \tag{11}$$

where $\varepsilon = [x_e, y_e]^T \in \mathbb{R}^2$, with x_e referred to as the along-track error and y_e as the cross-track error.

Taking the time derivative of ε, the error dynamics are given by:

$$\dot{\varepsilon} = \dot{R}^T(P_d - P_v) + R^T(\dot{P}_d - \dot{P}_v) \tag{12}$$

where:

$$\dot{R} = RS \tag{13}$$

and:

$$S = \begin{bmatrix} 0 & -\dot{\psi} \\ \dot{\psi} & 0 \end{bmatrix}, \quad \text{with } S = -S^T \tag{14}$$

The derivative of the desired path is:

$$\dot{P}_d = R_p \begin{bmatrix} U_d \\ 0 \end{bmatrix} \tag{15}$$

and:

$$\dot{P}_v = \dot{P} + \dot{R}E \tag{16}$$

From (13) and (13), the above equation can be rewritten as:

$$\dot{P}_v = R \begin{bmatrix} U \\ 0 \end{bmatrix} + RSE \tag{17}$$

where $U = \sqrt{u^2 + v^2}$ is the vehicle's resultant velocity. Substituting (13-17) into (12) yields:

$$\begin{aligned} \dot{\varepsilon} &= (RS)^T(P_d - P_v) + R^T\left(R_p \begin{bmatrix} U_d \\ 0 \end{bmatrix} - R\begin{bmatrix} U \\ 0 \end{bmatrix} - RS\begin{bmatrix} E_x \\ 0 \end{bmatrix}\right) \\ &= S^T\varepsilon + R^T R_p \begin{bmatrix} U_d \\ 0 \end{bmatrix} - R\begin{bmatrix} U \\ 0 \end{bmatrix} - S\begin{bmatrix} E_x \\ 0 \end{bmatrix} \end{aligned} \tag{18}$$

Expanding in scalar form:

$$\dot{x}_e = U_d(\cos(\psi - \gamma_d)\cos\beta - \sin(\psi - \gamma_d)\sin\beta) + \dot{\psi}y_e - U, \tag{19a}$$

$$\dot{y}_e = U_d(\sin(\psi - \gamma_d)\cos\beta + \cos(\psi - \gamma_d)\sin\beta) - \dot{\psi}x_e - E_x r \tag{19b}$$

The quantity $\beta = \text{atan2}(v, u)$ represents the sideslip angle, which arises from external disturbances or a non-zero sway velocity during a turn, causing a deviation in the vehicle's orientation ψ as explained in Pettersen and Nijmeijer (2001).

Assumption 5. In this work, the sideslip angle β is assumed to be small, such that $\sin\beta \approx \beta$ and $\cos\beta \approx 1$.

Remark 4. The Assumption 5 is widely adopted in the marine guidance literature (Fossen, 2023; Fossen et al., 2014; Martinović et al., 2024), since β is generally very low. This holds because typical AMVs are designed such that the sway velocity is much smaller than the surge velocity, making $\beta = atan2(v, u)$ naturally small. Moreover, the assumption simplifies the error dynamics without sacrificing accuracy and remains consistent with prior studies.

Under Assumption 5, equations (19) simplify to:

$$\dot{x}_e = U_d\cos(\psi - \gamma_d) - U_d\sin(\psi - \gamma_d)\beta + \dot{\psi}y_e - U \tag{20a}$$

$$\dot{y}_e = U_d\sin(\psi - \gamma_d) + U_d\cos(\psi - \gamma_d)\beta - \dot{\psi}x_e - E_x r \tag{20b}$$

The objective of the controller is to drive $x_e \to 0$ and $y_e \to 0$, aligning the vehicle's heading tangentially with the reference path. Accordingly, the desired heading ψ_d is defined as:

$$\psi_d = \gamma_d - \beta \tag{21}$$

Remark 5. Note that the sideslip angle β appears in both equations (20) and (21). However, β is an unknown quantity that must be estimated. Moreover, the attitude error dynamics $\dot{\psi}_e$ have not yet been explicitly addressed. These aspects will be discussed in the following sections.

4. Adaptive observer design

In this section, an AEKF-like observer is designed, inspired by (Martinović et al., 2024) to estimate the sideslip angle β. Although the design procedure is identical, the considered dynamics differ slightly.

To construct the adaptive observer, Eq. (20) is rewritten in a state-affine form:

$$\dot{\varepsilon} = A(t)\varepsilon + \varphi(t) + \Phi(t)\beta \tag{22a}$$

$$y = C\varepsilon \tag{22b}$$

where $\varphi(t) = [U_d\cos(\psi - \gamma_d) - U, U_d\sin(\psi - \gamma_d) - E_x r]^T$, $\Phi(t) = [-U_d\sin(\psi - \gamma_d), U_d\cos(\psi - \gamma_d)]^T$, $C = I_{2\times 2}$, and $A(t) = \begin{bmatrix} 0 & \dot{\psi} \\ -\dot{\psi} & 0 \end{bmatrix}$.

To ensure that the proposed AEKF observer accurately estimates the states and the sideslip angle β, the system is required to satisfy certain observability conditions. Specifically, the Uniform Observability Condition and the Persistent Excitation Condition are imposed.

Definition 1 (Uniform Observability Condition). (Besancon et al., 2006) The system (22) is said to satisfy uniform observability if there exist constants $0 < \alpha_1 < \sigma_1$ and $T_1 > 0$ such that:

$$\alpha_1 I \le \int_t^{t+T_1} \Psi(\tau)^T C^T \Sigma C \Psi(\tau) d\tau \le \sigma_1 I, \quad \forall t \ge t_0 \tag{23}$$

for some $t_0 \ge 0$ and a bounded positive definite matrix Σ, where $\Psi(t)$ is the transition matrix of the system: $\dot{\varepsilon} = A(t)\varepsilon$, $y = C\varepsilon$.

Definition 2 (Persistent Excitation Condition). (Besancon et al., 2006) The function $\Phi(t)$ is said to be persistently exciting if there exists a vector function $\Lambda(t)$, which is a solution of $\dot{\Lambda} = [A(t) - K(t)C(t)]\Lambda + \Phi(t)$, where $K(t)$ is a time-varying feedback gain that stabilizes the system (22). The function $\Lambda(t)$ satisfies the persistence excitation condition if there exist constants $0 < \alpha_2 < \sigma_2$ and $T_2 > 0$ such that:

$$\alpha_2 I \le \int_t^{t+T_2} \Lambda(\tau)^T C^T \Sigma C \Lambda(\tau) d\tau \le \sigma_2 I, \quad \forall t \ge t_0, \tag{24}$$

for some $t_0 \ge 0$ and a bounded positive definite matrix Σ.

Following (Besançon et al., 1996) and (Besancon et al., 2006), the AEKF is designed as follows:

$$\begin{aligned} \dot{\hat{\varepsilon}} &= A(t)\hat{\varepsilon} + \varphi(t) + \Phi(t)\hat{\beta} \\ &\quad + \left[\Lambda S_\beta^{-1}\Lambda^T C^T + S_\varepsilon^{-1}C^T\right]\Sigma(y - C\hat{\varepsilon}) \end{aligned} \tag{25a}$$

$$\dot{\hat{\beta}} = S_\beta^{-1}\Lambda^T C^T \Sigma(y - C\hat{\varepsilon}) \tag{25b}$$

$$\dot{\Lambda} = \left[A(t) - S_\varepsilon^{-1}C^T\Sigma C\right]\Lambda + \Phi(t) \tag{25c}$$

$$\dot{S}_\varepsilon = -\rho_x S_\varepsilon - A(t)^T S_\varepsilon - S_\varepsilon A(t) + C^T\Sigma C, \quad S_\varepsilon(0) > 0 \tag{25d}$$

$$\dot{S}_\beta = -\rho_\beta S_\beta + \Lambda^T C^T \Sigma C \Lambda, \; S_\beta(0) > 0 \tag{25e}$$

where $\hat{\varepsilon}$ and $\hat{\beta}$ denote the estimates of the tracking errors and the sideslip angle, respectively. The terms $\Lambda \in \mathbb{R}^2$, $S_\varepsilon \in \mathbb{R}^{2\times 2}$, and $S_\beta \in \mathbb{R}$ are adaptive gains with adaptive laws (25c)–(25e). ρ_ε and ρ_β are sufficiently large constants. The matrix Σ is a bounded positive definite matrix.

By defining $\tilde{\varepsilon} = \hat{\varepsilon} - \varepsilon$ and $\tilde{\beta} = \hat{\beta} - \beta$, Eqs. (25a) and (25b) can be written as:

$$\dot{\tilde{\varepsilon}} = \left(A(t) - \left[\Lambda S_\beta^{-1}\Lambda^T + S_\varepsilon\right]C^T\Sigma C\right)\tilde{\varepsilon} + \Phi(t)\tilde{\beta} \tag{26a}$$

$$\dot{\tilde{\beta}} = -S_\beta^{-1}\Lambda^T C^T \Sigma\tilde{\varepsilon} \tag{26b}$$

Remark 6. It can be verified that the considered system satisfies the conditions of uniform observability and persistence excitation. The function Ψ yields a rotation matrix, thus the term $\Psi^T C^T \Sigma C \Psi$ has the same eigenvalues as Σ. Since Σ is a bounded positive definite matrix the system satisfies the (23). The system (22), which is stabilized by $K = S_\varepsilon^{-1}C^T\Sigma C$, satisfies the upper bound of (24) since $\Phi(t)$ is bounded. For the lower bound, note that since the system is stable, $\dot{\Lambda} \approx \Phi$ for $t_0 > 0$. Since Φ is non zero at time $t > t_0$, Λ also remains nonzero. This ensures that $\Lambda^T C^T \Sigma C \Lambda$ remains positive definite, thereby satisfying the lower bound condition in (24).

Lemma 1. *Consider the adaptive observer defined by (25a)-(25e). If the system satisfies the Uniform Observability Condition (23) and the Persistent Excitation Condition (24), then the estimation errors $\tilde{\varepsilon} = \hat{\varepsilon} - \varepsilon$ and $\tilde{\beta} = \hat{\beta} - \beta$ are Uniformly Globally Exponentially Stable (UGES). Specifically, there exist positive constants $\underline{\sigma}, \overline{\sigma}, \rho > 0$ such that:*

$$\|\tilde{\varepsilon}(t)\|^2 + |\tilde{\beta}(t)|^2 \leq \frac{\overline{\sigma}}{\underline{\sigma}} e^{-\rho(t-t_0)}(\|\tilde{\varepsilon}(t_0)\|^2 + |\tilde{\beta}(t_0)|^2), \quad \forall t \geq t_0. \tag{27}$$

Proof. Refer to (Martinović et al., 2024) for a detailed proof. □

The results of Lemma 1 can be expressed more compactly by defining $\zeta = [\tilde{\varepsilon}^T \; \tilde{\beta}]^T \in \mathbb{R}^3$, as follows:

$$\|\zeta(t)\| \leq \sqrt{\frac{\overline{\sigma}}{\underline{\sigma}}} e^{-\frac{\rho}{2}(t-t_0)} \|\zeta(t_0)\| \tag{28}$$

This result establishes that the estimation errors $\tilde{\varepsilon}$ and $\tilde{\beta}$ decay exponentially to zero, ensuring the UGES of the adaptive observer. The rate of decay is governed by the parameter $\rho = min(\rho_\varepsilon, \rho_\beta)$, which depends on the observer gains. The parameters $\underline{\sigma}$ and $\overline{\sigma}$ denote the smallest and largest singular values of the matrix $diag(S_\varepsilon, S_\beta)$ The ratio $\frac{\overline{\sigma}}{\underline{\sigma}}$ quantifies how the initial estimation errors influence the convergence rate.

Theorem 1. *The observer error $\zeta(t)$ satisfy the exponential bound in (28) for all $t \geq t_0$, where $\rho > 0$ is the convergence rate and $\frac{\overline{\sigma}}{\underline{\sigma}}$ is a positive constant. Then, for any $k_{conv} > 0$ and sampling time $\delta > 0$, there exists a maximum estimation error bound $\zeta_{\max}$ such that:*

$$\|\zeta(t)\| \leq \zeta_{\max}, \quad \forall t \geq k_{conv}\delta, \tag{29}$$

where $k_{conv} > 0$ is a fixed number of sampling instants.

Proof. From Lemma 1, the observer error $\zeta(t)$ satisfies the exponential convergence bound as in (28). Fix any $k_{conv} > 0$ and sampling time $\delta > 0$, and consider that:

$$t = t_0 + k_{conv}\delta. \tag{30}$$

Substituting (30) into (28) yields the following expression:

$$\|\zeta(t_0 + k_{conv}\delta)\| \leq \sqrt{\frac{\overline{\sigma}}{\underline{\sigma}}} e^{-\frac{\rho}{2}k_{conv}\delta} \|\zeta(t_0)\|. \tag{31}$$

Now, defining the maximum estimation error bound as follows:

$$\zeta_{\max} := \sqrt{\frac{\overline{\sigma}}{\underline{\sigma}}} e^{-\frac{\rho}{2}k_{conv}\delta} \|\zeta(t_0)\|. \tag{32}$$

Since the right-hand side of (28) is monotonically decreasing in t, for all $t \geq t_0 + k_{conv}\delta$ it follows that:

$$\|\zeta(t)\| \leq \|\zeta(t_0 + k_{conv}\delta)\| \leq \zeta_{\max}. \tag{33}$$

This proves the existence of a finite bound $\zeta_{\max}$ such that

$$\|\zeta(t)\| \leq \zeta_{\max}, \quad \forall t \geq k_{conv}\delta, \tag{34}$$

completing the proof. □

5. Main results

In this section, the main results are presented. The solution to the path-following problem introduced in Section 3 is addressed using a two-stage control strategy as shown in Fig. 2. This strategy consists of an outer kinematic guidance loop that provides a reference velocity to an inner surge and yaw rate controller.

5.1. Kinematic guidance loop

The objective of the guidance loop is to drive both ε and ψ_e to zero. Previous studies employing the VRP approach have often overlooked the influence of the vehicle's attitude ψ in the path-following problem (Degorre et al., 2024a,b). In most cases, it is only shown that ψ remains bounded due to the system's internal dynamics (Matouš et al., 2024; Paliotta et al., 2018). However, in many marine vehicle applications such as docking and station keeping, large deviations in ψ can lead to mission failure or safety violations

To address this, the error dynamics of ψ_e, defined as $\psi_e = \psi_d - \psi$, are considered. Its time derivative is given by:

$$\dot{\psi}_e = \dot{\psi}_d - r \tag{35}$$

where ψ_d is defined in Eq. (21). In Eq. (21), β is an unknown parameter that is estimated as $\hat{\beta}$ using the adaptive observer as in (25).

Eqs. (35) and (20) together yield the complete error dynamics, expressed as follows:

$$\dot{x}_e = r y_e + U_d \cos(\psi_e) - U \tag{36a}$$
$$\dot{y}_e = -r x_e + U_d \sin(\psi_e) - r E_x \tag{36b}$$
$$\dot{\psi}_e = \dot{\psi}_d - r \tag{36c}$$

At this point, the advantages of the proposed virtual point guidance method are highlighted. In traditional LOS guidance, y_e is minimized by selecting an appropriate heading reference $\psi_d(y_e)$. However, with virtual point guidance, y_e can be directly influenced through r, as it explicitly appears in (36b). Furthermore, ψ_e is also regulated via r, meaning that both errors are minimized using the same virtual input. This coupling necessitates an optimal control approach to balance their simultaneous reduction.

To accomplish this, a NMPC framework is employed. This framework optimally adjusts r while respecting system constraints, offering improved performance. Moreover, the NMPC formulation is integrated with a Controlled Lyapunov Function (CLF) to retain global stability guarantees, following the approach in Grandia et al. (2020).

Since the sideslip angle β is not directly measurable, the estimation $\hat{\beta}$ by the AEKF is used in the error dynamics, forming the basis for the NMPC problem. Thus, the NMPC optimization relies on the estimated state vector $\hat{\chi}(t_i) \in \mathbb{R}^3$ at time t_i. While not all states need to be estimated, the NMPC uses the available estimates to achieve optimal performance while maintaining constraint adherence.

To formulate the CLF-based NMPC (LNMPC), the error dynamics in equation (36) are rewritten compactly as:

$$\dot{\chi} = f(\chi, \upsilon), \tag{37}$$

where $\chi = [x_e, y_e, \psi_e]^T \in \mathbb{R}^3$ is the state vector, and $\upsilon = [u, r]^T \in \mathbb{R}^2$ is the virtual control input.

Remark 7. In earlier formulations, the resultant velocity was expressed as $U = \sqrt{u^2 + v^2}$. However, since the sway velocity v is not directly actuated and the vehicle predominantly travels tangent to the desired path, it holds that $U \approx u$, i.e., the resultant velocity is well approximated by the surge velocity (Degorre et al., 2024b). Consequently, in this work U is replaced with u to ensure consistency with the physically actuated input. This substitution does not compromise the validity of the subsequent stability analysis or control design.

Assumption 6. The function $f(\chi, \upsilon)$ is assumed to be locally Lipschitz continuous in both χ and υ on a domain containing the origin. Specifically, there exists a constant $L > 0$ such that for all $\chi_1, \chi_2 \in \mathbb{R}^3$ and $\upsilon_1, \upsilon_2 \in \mathbb{R}^2$:

$$\|f(\chi_1, \upsilon_1) - f(\chi_2, \upsilon_2)\| \leq L\|\chi_1 - \chi_2\| \tag{38}$$

where L is the Lipschitz constant associated with $f(\chi, \upsilon)$. The origin is an equilibrium point for the nominal system, i.e., $f(0, 0) = 0$.

Given the error system (37) and the adaptive observer (25), the open-loop optimization problem at each time instant t_i $(i \geq 0)$ is formulated as:

$$\min_{\bar{\upsilon}(\cdot)} J\left(\hat{\chi}(t_i), \bar{\upsilon}(\cdot)\right) = \int_{t_i}^{t_i+T_p} \left(\|\bar{\chi}(t_i, \tau)\|_Q^2 + \|\bar{\upsilon}(t_i, \tau)\|_R^2\right) d\tau \tag{39a}$$

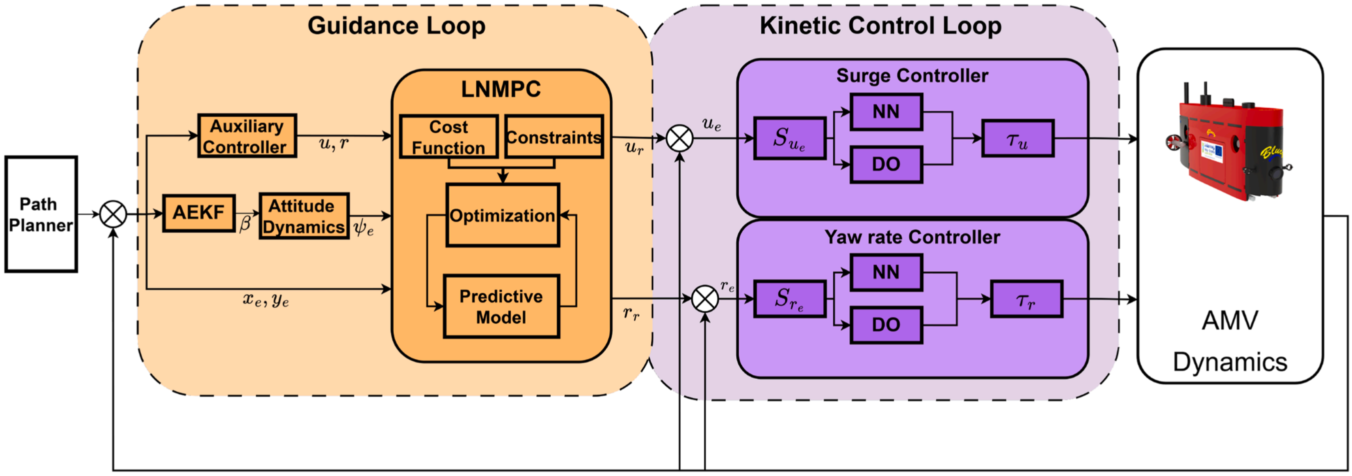

Fig. 2. Block diagram of the proposed two-stage control architecture. The outer LNMPC based kinematic guidance loop generates reference signals for the inner surge and yaw rate controller.

subject to:

$$\dot{\bar{\chi}}(\tau) = f(\bar{\chi}(t_i,\tau), \bar{v}(t_i,\tau)), \tag{39b}$$

$$\bar{\chi}(t_i) = \hat{\chi}(t_i) \tag{39c}$$

$$\bar{v}(\tau) \in \mathcal{U}, \tag{39d}$$

$$\frac{\partial V_1}{\partial \chi} f(\bar{\chi}(t_i,\tau), \bar{v}(\hat{\chi}(t_i),\tau)) \le \frac{\partial V_1}{\partial \chi} f(\bar{\chi}(t_i,\tau), \tilde{v}(\hat{\chi}(t_i),\tau)) \tag{39e}$$

The objective is to minimize the cost function J, which includes a weighted sum of the state error and control effort over the prediction horizon T_p. The function $f(\bar{\chi},\bar{v})$ describes the system dynamics, while $\bar{\chi}(t_i,\tau)$ and $\bar{v}(t_i,\tau)$ denote predicted state and input trajectories. The matrices Q, R, and P are positive definite weights penalizing state deviation, control effort, and terminal error, respectively. The control constraint set is defined as $\mathcal{U} = \{v \in \mathbb{R}^2 \mid v_{\min} \le v_i \le v_{\max}\}$ for $i = 1, 2$. Here, $V_1(\cdot)$ is the CLF, and $\tilde{v}$ is the auxiliary controller ensuring satisfaction of the constraint (39e), presented in the later part of this section.

At each sampling instant, the LNMPC solves the optimization problem to determine the optimal control sequence. Based on the observer-estimated state $\hat{\chi}$, the system's future behavior is predicted using $f(\bar{\chi},\bar{v})$. After solving the optimization problem, only the first control input $\bar{v}^*(\cdot,\hat{\chi}(t_i))$ is applied. This receding horizon approach enhances robustness against model uncertainty and external disturbances.

Auxiliary Lyapunov based controller

To design the auxiliary controller introduced in the LNMPC problem is addressed here. Let the Lyapunov function be defined as:

$$V_1(\chi) = \frac{1}{2}(x_e^2 + y_e^2) \tag{40}$$

Taking the time derivative of V_1 along the system dynamics yields:

$$\dot{V}_1 = x_e\dot{x}_e + y_e\dot{y}_e \tag{41}$$

Substituting the system dynamics, we obtain:

$$\begin{aligned}\dot{V}_1 &= x_e(\dot{\psi} y_e + U_d\cos(\psi_e) - U)\\ &\quad + y_e(-\dot{\psi} x_e + U_d\sin(\psi_e) - rE_x)\end{aligned} \tag{42}$$

Now by choosing the feedback control law $\tilde{u} = [U, r]^T$ given as:

$$u = U_d\cos\psi_e + k_1 x_e \tag{43a}$$

$$r = \frac{U_d\sin\psi_e + k_2 y_e}{E_x} \tag{43b}$$

Finally, substituting the control law (43) in $\dot{V}_1$ we obtain:

$$\begin{aligned}\dot{V}_1 &= -k_1x_e^2 - k_2y_e^2\\ &= -\alpha V_1\end{aligned} \tag{44}$$

where α is $\min(\frac{k_1}{2}, \frac{k_2}{2})$. Thus, if $k_1 > 0$ and $k_2, > 0$ any states $\chi \in \mathcal{W}$ (will be defined later), the system states remain bounded and asymptotically converge to equilibrium.

Note that ψ_e is not included in the Lyapunov function. This is because orientation error ψ_e remains bounded under the proposed control law, even though it is not directly included in the Lyapunov function. From the closed-loop dynamics, we have

$$\dot{\psi}_e = \dot{\psi}_d - r = \dot{\psi}_d - \frac{U_d\sin\psi_e + k_2y_e}{E_x} \tag{45}$$

where $\dot{\psi}_d$ is the desired angular rate and it is bound such that there exits a $|\dot{\psi}_d(t)| \le \dot{\psi}_d^{\max}$. Define the auxiliary function $V_2 = 1 - \cos\psi_e$, which is positive definite and radially unbounded with respect to ψ_e. Taking the time derivative yields

$$\dot{V}_2 = \sin\psi_e \cdot \dot{\psi}_e = \sin\psi_e\left(\dot{\psi}_d - \frac{U_d\sin\psi_e + k_2y_e}{E_x}\right) \tag{46}$$

This simplifies to

$$\dot{V}_2 = \dot{\psi}_d\sin\psi_e - \frac{U_d}{E_x}\sin^2\psi_e - \frac{k_2}{E_x}y_e\sin\psi_e. \tag{47}$$

Since $\dot{\psi}_d$ is bounded and $y_e(t) \to 0$ as $t \to \infty$, the last term vanishes asymptotically. For sufficiently large t, $\dot{V}_2$ is bounded by

$$\dot{V}_2 \le \dot{\psi}_d^{\max}|\sin\psi_e| - \frac{U_d}{E_x}\sin^2\psi_e \tag{48}$$

This expression defines a concave quadratic in $|\sin\psi_e|$ with a maximum, implying that for large enough ψ_e, the dissipative term dominates, and $\dot{V}_2 < 0$. Thus, $V_2(t)$ cannot increase indefinitely, and $\psi_e(t)$ must remain bounded. Therefore, under the proposed control law, the heading error ψ_e remains bounded for all time.

Now the level set, where the system is expected to converge, is chosen as:

$$\mathcal{W}_C = \{(x_e, y_e, \psi_e) \mid V_1(\chi) \le C\} \tag{49}$$

If the proposed controllers (43) satisfy the input constraints $\mathcal{U}$, then the upper bound on δ is given by:

$$C \le \min\left(\frac{(u_{\max} - U_d\cos(\psi_e))^2}{2k_1^2}, \frac{(r_{\max}E_x - U_d\sin\psi_e)^2}{2k_2^2}\right) \tag{50}$$

The choice of the level set $\mathcal{W}$ is crucial because it ensures recursive feasibility, provided disturbances remain within allowable bounds.

Stability of the LNMPC

The stability of the closed-loop LNMPC combined with an AEKF observer is based on the existence of a continuous value function that remains inherently robust to the state estimation error introduced by the AEKF. This estimation error acts as a disturbance in the closed-loop system but does not destabilize it as proven in the following theorem.

Theorem 2. *Consider the error dynamics (37) subject to the LNMPC scheme defined in (39), where the estimated state $\hat{\chi}(t)$ is provided by an AEKF. Suppose the following conditions hold:*

- *The true system dynamics satisfy the Lipschitz continuity condition stated in Assumption 6.*
- *There exists a control Lyapunov function $V_1(\chi)$ satisfying the CLF condition (39e) under the auxiliary control law (43), within the set $\mathcal{W}_C = \{(x_e, y_e, \psi_e) \mid V_1(\chi) \le C\}$.*
- *The observer satisfies the bounded estimation error condition $\|\chi(t_i) - \hat{\chi}(t_i)\| \le \zeta_{\max}$ for all $t_i \ge K_{conv}\delta$, where K_{conv} denotes the observer convergence time.*

Then, for all sampling times $\delta \le \delta_{\max}$ and estimation error bounds $\zeta \le \zeta_{\max}$ satisfying the bounds (52) and (60), the following properties hold:

1. ***(Recursive Feasibility)** The LNMPC optimization problem remains feasible at all sampling instants t_i.*
2. ***(Convergence)** For any initial condition $\chi(0) \in \mathcal{W}_{C_0} \subset \mathcal{W}_C$, the closed-loop trajectory $\chi(t)$ converges to the set $\mathcal{W}_{\alpha/2} \subset \mathcal{W}_\alpha \subset \mathcal{W}_C$, and remains within $\mathcal{W}_\alpha$ thereafter.*

Proof. Step 1: Recursive Feasibility: Consider any sampling instant t_i at which a feasible solution exists i.e., $(\bar{\upsilon}^*(\cdot, \chi(t_i)))$, meaning the LNMPC problem has an optimal solution that ensures both constraint satisfaction and proper system dynamics evolution.

Between t_i and t_{i+1}, the control input applied to the system is $\bar{\upsilon}^*(\cdot, \chi(t_i))$. The remainder of the optimal input sequence, $\bar{\upsilon}^*(\tau, \chi(t_i))$, for $\tau \in [t_{i+1}, t_i + T_p]$, continues to satisfy the system constraints. Furthermore, for all $\chi(t_i + T_p) \in \mathcal{W}_C$, there exists an auxiliary control law $\tilde{\upsilon}(\cdot)$ such that the CLF condition (39e) and the control constraint (39d) are satisfied. For any time $t_i + \sigma$, where $\sigma \in (0, t_{i+1} - t_i]$, the control input is defined as:

$$\bar{\upsilon}(\tau, \chi(t_i + \sigma)) = \begin{cases} \bar{\upsilon}^*(\tau, \chi\hat{(}t_i)), & \text{for } \tau \in [t_{i+1}, t_i + T_p], \\ \tilde{\upsilon}(\tau - t_i - T_p), & \text{for } \tau \in (t_i + T_p, t_i + T_p + \sigma]. \end{cases} \tag{51}$$

Since $\bar{\upsilon}(\cdot, \chi(t_{i+1}))$ satisfies all state and input constraints and preserves the CLF condition due to the terminal auxiliary control law $\tilde{\upsilon}$, recursive feasibility of the LNMPC optimization problem at time t_{i+1} is guaranteed.

Step 2: Convergence The convergence is proven in two parts.

Part one: For any initial state $\chi(0) \in \mathcal{W}_{C_0}$, which is strictly contained within $\mathcal{W}_C$, the state will reach a set $\mathcal{W}_{C_1}$ where $C_1 = C_0 + (C - C_0)/2$ after some $T_{C_0C_1}$. The existence of such a $T_{C_0C_1}$ is guaranteed under the assumption (6), because $\forall \chi(\tau) \in \mathcal{W}_C$ then, we have $\|\chi(\tau) - \chi(0)\| \le \int_0^\tau \|f(\chi(t), \upsilon(t))\| dt \le K_{\mathcal{W}_C} t$ where the $K_{\mathcal{W}_C}$ is a constant depending on the Lipschitz constant of $f(\chi, \upsilon)$ and the bound on υ. Let $T_{C_0C_1}$ be the minimum time required to reach the boundary of $\mathcal{W}_{C_1}$, from any point $\chi(0) \in \mathcal{W}_{C_0}$ allowing $\upsilon(t)$ to take admissible values in $\mathcal{U}$. By similar arguments, there also exists a time T_{C_2C} such that for all $\chi(t_i) \in \mathcal{W}_{C_2}$, the state $\chi(\tau) \in \mathcal{W}_C$ for all $\tau \in [t_i, t_i + T_{C_2C})$. where $C_2 = C_1 + (C - C_1)/2$. We now pick the maximum sampling time $\delta_{\max}$ as

$$\delta_{max} = \min\left\{T_{C_0C_1}/k_{Conv}, T_{C_2C}\right\} \tag{52}$$

Thus, any initial state in $\mathcal{W}_{C_0}$ does not leave the level set $\mathcal{W}_C$ during the convergence of observer $K_{\text{conv}}\delta_{\max}$.

Part two: Since the Lyapunov function $V_1(\chi)$ is continuously differentiable and radially unbounded, we can apply converse Lyapunov theorems there exists a functions β_1, β_2 and β_3 that belongs to $\mathcal{K}_\infty$ such that the following inequalities hold:

$$\beta_1(\|\chi\|) \le V_1(\chi) \le \beta_2(\|\chi\|) \tag{53a}$$

$$\frac{\partial V_1}{\partial \chi} f(\chi, \tilde{\upsilon}) \le -\beta_3(\|\chi\|) \tag{53b}$$

Furthermore from the (39e) and (39d) we have the following inequality:

$$\begin{aligned} \frac{\partial V_1}{\partial \chi} f(\bar{\chi}(t_i, \tau), \bar{\upsilon}^*(\hat{\chi}(t_i), \tau)) &\le \frac{\partial V_1}{\partial \chi} f(\bar{\chi}(t_i, \tau), \tilde{\upsilon}(\hat{\chi}(t_i), \tau)) \\ &\le -\beta_3(\|\chi\|) \end{aligned} \tag{54}$$

Now, for any $\chi(t_i) \in \mathcal{W}_{C_1}$, the time derivative of the Lyapunov function along the trajectory state trajectory $\chi(\tau)$ of the system, $\forall \tau \in [t_i, t_i + 1)$

$$\dot{V}_1(\chi(\tau)) = \frac{\partial V_1}{\partial \chi} f(\chi(\tau), \bar{\upsilon}^*(\hat{\chi}(t_i), \tau)) \tag{55}$$

By adding and subtracting the term $\frac{\partial V_1}{\partial \chi} f(\bar{\chi}(t_i, \tau), -\bar{\upsilon}^*(\hat{\chi}(t_i), \tau))$ and taking (54) into consideration, one gets:

$$\begin{aligned} \dot{V}_1(\chi(\tau)) = &\frac{\partial V_1}{\partial \chi} f(\chi(\tau), \bar{\upsilon}^*(\hat{\chi}(t_i), \tau)) \\ &+ \frac{\partial V_1}{\partial \chi} f(\bar{\chi}(t_i, \tau), \bar{\upsilon}^*(\hat{\chi}(t_i), \tau)) \\ &- \frac{\partial V_1}{\partial \chi} f(\bar{\chi}(t_i, \tau), \bar{\upsilon}^*(\hat{\chi}(t_i), \tau)) \\ = &-\beta_3(\|\chi\|) + \frac{\partial V_1}{\partial \chi} f(\chi(\tau), \bar{\upsilon}^*(\hat{\chi}(t_i), \tau)) \\ &- \frac{\partial V_1}{\partial \chi} f(\bar{\chi}(t_i, \tau), \bar{\upsilon}^*(\hat{\chi}(t_i), \tau)) \end{aligned} \tag{56}$$

Since function $f(\chi, \upsilon)$ is Lipschitz continuous (Assumption 6) and V_1 is continuously differentiable, then $\frac{\partial V_1}{\partial x} f(\cdot)$ is also Lipschitz. Thus we have:

$$\dot{V}_1(\chi(\tau)) = -\beta_3(\|\chi\|) + L_V \left\|\chi(\tau) - \bar{\chi}(t_i, \tau)\right\| \tag{57}$$

here, L_V is the Lipschitz constant associated with $\frac{\partial V_1}{\partial \chi} f(\chi, \upsilon)$.

The prediction error between $\chi(\tau)$ and $\bar{\chi}(t_i, \tau)$ is related to the state estimation error and it can be bounded using the Grönwall-Bellman inequality as follows:

$$\left\|\chi(\tau) - \bar{\chi}(t_i, \tau)\right\| \le e^{L_f \tau} \left\|\chi(t_i) - \hat{\chi}(t_i)\right\| \tag{58}$$

where L_f is the Lipschitz constant associated with $f(\cdot)$. We thus obtain the bound on $\dot{V}_1(\chi(\tau))$:

$$\dot{V}_1(\chi(\tau)) = -\beta_3(\|\chi\|) + L_V e^{L_f \tau} \left\|\chi(t_i) - \hat{\chi}(t_i)\right\| \tag{59}$$

Now assuming that $x(\tau) \notin \mathcal{W}_{\alpha/2}$ i.e., $\|\chi\| \ge \alpha/2$ and since $\beta_3 \in K_\infty$, we have $\beta_3(\|\chi\|) \ge \beta_3(\alpha/2)$. Hence for any χ to converge to the set $\mathcal{W}_{\alpha/2}$, From Theorem 1, there exists a bound $|\chi(t_i) - \hat{\chi}(t_i)| \le \zeta_{\max}$, and the observer parameter $\zeta_{\max}$ should be chosen such that:

$$L_V(e^{L_f \tau} \zeta_{max}) \le \beta_3(\alpha/2) \tag{60}$$

where $e_{\max}$ the maximum estimation error after the convergence time $K_{conv}\delta$.

Integrating both sides over the interval $[t_i, t_i + 1]$, we get:

$$V_1(\chi(t_i + 1)) - V_1(\chi(t_i)) \le -\beta_3(\alpha/2) \tag{61}$$

which implies:

$$V_1(\chi(t_i + 1)) \le V_1(\chi(t_i)) - \beta_3(\alpha/2) \tag{62}$$

By recursively applying the inequality, we conclude that if any $\chi(0) \in \mathcal{W}_{C_0}$ will converge to $\mathcal{W}_{\alpha/2}$ in a finite time without leaving the admissible set $\mathcal{W}_C$ if the observer parameters satisfies (52) and (60). Once the system reaches $\mathcal{W}_{\alpha/2}$, it will remain inside $\mathcal{W}_\alpha$. this statement holds because the $\mathcal{W}_{\alpha/2} \subseteq \mathcal{W}_\alpha$. □

5.2. Kinetic control loop

At the kinetics level, the virtual desired velocities generated by the guidance stage are tracked by designing the input thrusts. To achieve this, we employ a neural adaptive sliding mode control strategy as proposed in Menghini et al. (2024a). We define the tracking errors as $u_e = u - u_r$ and $r_e = r - r_r$, and introduce the following sliding surfaces:

$$s_{u_e} = u_e + \lambda_{u_e} \int u_e \, dt \tag{63a}$$

$$s_{r_e} = r_e + \lambda_{r_e} \int r_e \, dt \tag{63b}$$

where $\lambda_{(\cdot)}$ are positive design constants. The time derivatives of the sliding surfaces are given by:

$$\begin{aligned} \dot{s}_{u_e} &= \dot{u}_e + \lambda_{u_e} u_e \\ &= f_u(u, v, r) + \Delta_{f_u} + \tau_u + d_u - \dot{u}_r + \lambda_{u_e} u_e \end{aligned} \tag{64a}$$

$$\begin{aligned} \dot{s}_{r_e} &= \dot{r}_e + \lambda_{r_e} r_e \\ &= f_r(u, v, r) + \Delta_{f_r} + \tau_r + d_r - \dot{r}_r + \lambda_{r_e} r_e \end{aligned} \tag{64b}$$

where $\Delta_{(\cdot)}$ represent model uncertainties and unmodeled dynamics. These uncertainties are approximated using Radial Basis Function Neural Networks (RBF-NNs) as $\hat{\Delta}_{(\cdot)} = \hat{W}_{(\cdot)} \mu_{(\cdot)}$, where $\hat{W}_{(\cdot)}$ are the estimated neural network weights, and $\mu_{(\cdot)}$ are Gaussian basis functions. The weight estimation error is denoted by $\tilde{W}_{(\cdot)} = \hat{W}_{(\cdot)} - W^*_{(\cdot)}$, where W^* are the ideal weights.

To enforce convergence, the sliding surface dynamics are designed to follow the following reaching law:

$$\dot{s}_{u_e} = -k_{u_e} s_{u_e} - D_{u_e} sign(s_{u_e}) \tag{65a}$$

$$\dot{s}_{r_e} = -k_{r_e} s_{r_e} - D_{r_e} sign(s_{r_e}) \tag{65b}$$

where $k_{(\cdot)}$ are positive gains and $D_{(\cdot)}$ are disturbance compensation terms. These are estimated adaptively to account for external disturbances $d_{(\cdot)}$ and approximation errors of the neural network. Let $\hat{D}_{(\cdot)}$ denote the estimates of these terms, and $\tilde{D}_{(\cdot)} = \hat{D}_{(\cdot)} - d_{(\cdot)}$ their estimation errors.

By combining (64) and (65), the control inputs τ_u and τ_r are designed to enforce the reaching law as follows:

$$\tau_u = -f_u(u, v, r) - \hat{\Delta}_{f_u} + \dot{u}_r - \lambda_{u_e} u_e - k_{u_e} s_{u_e} - \hat{D}_{u_e} sign(s_{u_e}) \tag{66a}$$

$$\tau_r = -f_r(u, v, r) - \hat{\Delta}_{f_r} + \dot{r}_r - \lambda_{r_e} r_e - k_{r_e} s_{r_e} - \hat{D}_{r_e} sign(s_{r_e}) \tag{66b}$$

Stability of the control loop

To analyze the stability of the proposed adaptive sliding mode controller, we define a Lyapunov function candidate as:

$$\begin{aligned} V =& \frac{1}{2} s_{u_e}^2 + \frac{1}{2} s_{r_e}^2 + \frac{1}{2} \mathrm{tr}\left(\tilde{W}_u^\top \Gamma_u^{-1} \tilde{W}_u\right) + \frac{1}{2} \mathrm{tr}\left(\tilde{W}_r^\top \Gamma_r^{-1} \tilde{W}_r\right) \\ &+ \frac{1}{2} \tilde{D}_{u_e}^2 + \frac{1}{2} \tilde{D}_{r_e}^2 \end{aligned} \tag{67}$$

$\Gamma_{(\cdot)}$ are positive-definite learning rate matrices.

Taking the time derivative of V yields:

$$\begin{aligned} \dot{V} =& s_{u_e} \dot{s}_{u_e} + s_{r_e} \dot{s}_{r_e} + \mathrm{tr}\left(\tilde{W}_u^\top \Gamma_u^{-1} \dot{\hat{W}}_u\right) + \mathrm{tr}\left(\tilde{W}_r^\top \Gamma_r^{-1} \dot{\hat{W}}_r\right) \\ &+ \tilde{D}_{u_e} \dot{\hat{D}}_{u_e} + \tilde{D}_{r_e} \dot{\hat{D}}_{r_e} \end{aligned} \tag{68}$$

Using the error dynamics and control laws from Eq. (64) and Eq. (65), we substitute:

$$\dot{s}_{u_e} = -k_{u_e} s_{u_e} - D_{u_e} \mathrm{sign}(s_{u_e}) + \tilde{\Delta}_{f_u} + \tilde{D}_{u_e} \mathrm{sign}(s_{u_e}) \tag{69}$$

$$\dot{s}_{r_e} = -k_{r_e} s_{r_e} - D_{r_e} \mathrm{sign}(s_{r_e}) + \tilde{\Delta}_{f_r} + \tilde{D}_{r_e} \mathrm{sign}(s_{r_e}) \tag{70}$$

Substituting these into $\dot{V}$:

$$\begin{aligned} \dot{V} =& -k_{u_e} s_{u_e}^2 - k_{r_e} s_{r_e}^2 + s_{u_e} \tilde{\Delta}_{f_u} + s_{r_e} \tilde{\Delta}_{f_r} + \tilde{D}_{u_e} |s_{u_e}| \\ &+ \tilde{D}_{r_e} |s_{r_e}| + \mathrm{tr}\left(\tilde{W}_u^\top \Gamma_u^{-1} \dot{\hat{W}}_u\right) + \mathrm{tr}\left(\tilde{W}_r^\top \Gamma_r^{-1} \dot{\hat{W}}_r\right) \\ &+ \tilde{D}_{u_e} \dot{\hat{D}}_{u_e} + \tilde{D}_{r_e} \dot{\hat{D}}_{r_e} \end{aligned} \tag{71}$$

To cancel the NN approximation and disturbance terms, we define the adaptive update laws:

$$\dot{\hat{W}}_u = \Gamma_u s_{u_e} \mu_u \tag{72a}$$

$$\dot{\hat{W}}_r = \Gamma_r s_{r_e} \mu_r \tag{72b}$$

$$\dot{\hat{D}}_{u_e} = \gamma_{D_u} |s_{u_e}| \tag{72c}$$

$$\dot{\hat{D}}_{r_e} = \gamma_{D_r} |s_{r_e}| \tag{72d}$$

Substituting these into the Lyapunov derivative leads to:

$$\dot{V} = -k_{u_e} s_{u_e}^2 - k_{r_e} s_{r_e}^2 \le 0 \tag{73}$$

Since $\dot{V} \le 0$, the Lyapunov function is non-increasing and bounded below. Thus, sliding surface is asymptotically stable, i.e,

$$\lim_{t\to\infty} s_{u_e}(t) = 0, \quad \lim_{t\to\infty} s_{r_e}(t) = 0 \tag{74}$$

Because of (63), we also have:

$$\lim_{t\to\infty} u_e(t) = 0, \quad \lim_{t\to\infty} r_e(t) = 0 \tag{75}$$

Therefore, the proposed controller guarantees that all signals remain bounded, and the tracking errors asymptotically converge to zero in the presence of modeling uncertainty and bounded external disturbances.

Remark 8. Note that the sway dynamics (v), are not explicitly included in the stability analysis. However, it can be shown that v remains uniformly bounded for any $Y_1, Y_2 \ge 0$ in (4b), provided that the surge velocity u, yaw rate r, and disturbance d_v are bounded, as demonstrated in Pettersen and Egeland (2002). Moreover, most AMVs are designed such that the conditions $Y_1, Y_2 \ge 0$ are naturally satisfied (see Remark 3 in Paliotta et al. (2018)).

Remark 9. The overall stability of the closed-loop system, comprising both the guidance loop and the kinetic control loop discussed above, can be analyzed using singular perturbation theory (See Khalil & Grizzle, 2002, Chapter. 11). In this framework, the control loop operates on a faster timescale compared to the guidance loop, owing to the relative separation in their dynamic responses. By treating the guidance system as a slow subsystem and the control dynamics as a fast subsystem, one can demonstrate that the composite system remains stable under the Tikhonov theorem conditions (See Khalil & Grizzle, 2002, Chapter. 11, Section 2). This entails proving that both the reduced slow system and the boundary-layer fast system are stable in isolation and that the fast subsystem converges quickly to a quasi-steady state. However, for brevity, this detailed analysis is omitted here as the primary focus of this work is on the VRP-based guidance strategy.

6. Case study: Blucy

Blucy is an underactuated underwater vehicle used for non-invasive underwater monitoring. The vehicle is equipped with six thrusters, as shown in Fig. 3: two longitudinal thrusters for surge, two lateral thrusters for yaw control, and two vertical thrusters for depth and heave control without inducing pitch. Although sway can be influenced using the lateral thrusters, the vehicle's design makes direct sway control inefficient, as overcoming the hydrodynamic drag in this direction requires significantly more thrust due to the large lateral surface area exposed.

The pitch and roll dynamics are inherently stable due to hydrostatic restoring forces resulting from the vertical offset between the center of gravity (CoG) and the center of buoyancy (CoB). This design satisfies all assumptions outlined in Section 2 for the 3-DOF planar motion model. The physical parameters of the vehicle were experimentally identified and validated by the authors in Menghini et al. (2024b). Hence, although the results presented here are based on simulations, they are grounded in experimentally validated dynamics,

Fig. 3. Blucy underwater vehicle with 6-thruster configuration.

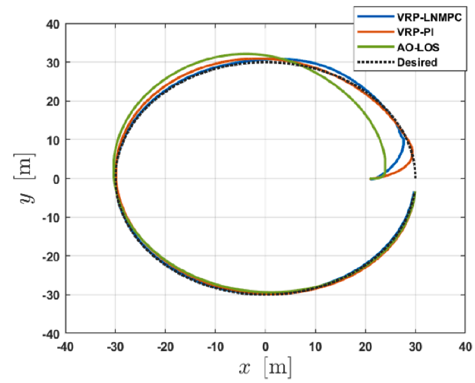

Fig. 4. Vehicle trajectories under a constant sea current. The comparison illustrates the path-following performance of the PI, LNMPC, and AO-LOS controllers.

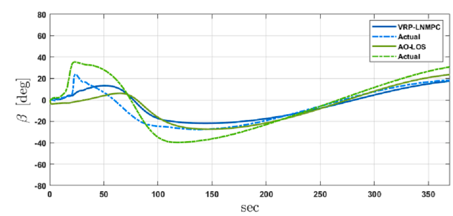

Fig. 5. Estimated sideslip angle $\hat{\beta}$ obtained from the AEKF under constant current conditions.

6.1. *Simulation results*

The proposed guidance and control framework is implemented and evaluated in a MATLAB/Simulink environment. The performance of the LNMPC-based guidance strategy is compared against two baseline methods: the VRP-PI controller, which employs a proportional–integral kinematic structure, and the Adaptive Observer–based Line-of-Sight (AO-LOS) controller, as presented in Degorre et al. (2024a) and Martinović et al. (2024), respectively.

To ensure a fair and systematic comparison, all controllers are evaluated using the same reference path and identical initial conditions. The analysis is carried out under two different environmental conditions: (i) a constant current scenario, and (ii) a time-varying current scenario, introduced to assess robustness against external disturbances.

6.1.0.1. Parameter Settings:. The observer and controller parameters used in the simulations are as follows: The adaptive observer parameters are $\rho_z = 5$, $\rho_\beta = 0.05$, and $\Sigma = 1.2 I_{2\times2}$. The LNMPC parameters include the sampling period $\delta = 0.1$, the prediction horizon $T_p = 5$, the weight matrices $Q = \mathrm{diag}(5, 5, 8)$ and $R = \mathrm{diag}(1.2, 1.2)$, the input limits $u = [0, 1]$ m/s and $r = [-0.2, 0.2]$ rad/s, and the auxiliary control gains $k_1 = 0.8$ and $k_2 = 1$. The control loop parameters are $\lambda_{u_e} = 0.1$, $\lambda_{r_e} = 0.2$, $\gamma_{D_u} = 3$, $\gamma_{D_r} = 5$, $\Gamma_u = 10$, and $\Gamma_r = 10$. The virtual reference point is set to $E_x = 0.8$ m and $E_y = 0$. For the VRP-PI controller, the proportional gains are $P_{x_e} = 1$ and $P_{y_e} = 1$, while the integral gains are $I_{x_e} = 0.01$ and $I_{y_e} = 0.01$. Finally, the AO-LOS control parameters are the look-ahead distance $\Delta = 3$ and the velocity control gain $K_{x_e} = 2.5$.

6.1.0.2. Reference Path Description:. All simulations are conducted using a single curved reference path defined as a circular arc in the horizontal plane. The path is parametrized as

$$x(\varsigma) = R\cos(\varsigma), \tag{76}$$

$$y(\varsigma) = R\sin(\varsigma), \tag{77}$$

where $R = 30$ m denotes the radius of curvature and ς is the path parameter.

The vehicle is initialized at position $(x_0, y_0) = (20 \text{ m}, 0 \text{ m})$ with an initial heading of $\psi_0 = 0°$. The initial surge velocity and yaw rate are set to $u_0 = 0$ m/s and $r_0 = 0$ rad/s, respectively. The total simulation time is 370 s.

6.1.0.3. (i) Constant Current:. In this first scenario, the vehicle is subjected to a constant sea current in order to evaluate nominal tracking performance under steady environmental conditions. The sea current is modeled as a uniform and constant velocity field expressed in the inertial frame. The current magnitude is set to $V_c = 0.3$ m/s, with a fixed direction of 30°, corresponding to a current acting along the x-axis of the inertial frame. This scenario represents operating conditions in which environmental disturbances are approximately constant over the mission duration, such as in regions with steady tidal flow or weak sea currents.

Fig. 4 illustrates the vehicle trajectories under a constant sea current of 0.3 m/s for both the PI and LNMPC controllers. Although both controllers achieve bounded tracking along the reference path, clear differences appear in how the disturbance is handled and compensated.

For the PI controller, the vehicle converges to a steady-state motion characterized by a constant heading offset relative to the path tangent. This behavior is expected, since the PI controller does not explicitly regulate attitude. Instead, the heading evolves according to the vehicle dynamics and settles to an equilibrium that balances the external current, resulting in a nonzero crab angle and small but persistent lateral tracking errors, as shown in Fig. 6.

In contrast, the LNMPC explicitly incorporates attitude regulation into the control objective. As shown in Fig. 5, the heading is regulated with respect to the reference $\gamma_d - \hat{\beta}$, where $\hat{\beta}$ is provided by the AEKF. Unlike the instantaneous kinematic computation $\beta = \arctan(v/u)$, the estimated sideslip is reconstructed from the system dynamics and tracking errors. Consequently, $\hat{\beta}$ exhibits a transient phase lag, particularly during changes in the disturbance.

This observer-induced phase lag is not detrimental; instead, it acts as an implicit filtering mechanism that avoids high-frequency oscillations that may arise from directly feeding back $\beta = \arctan(v/u)$. As a result, the LNMPC maintains smooth and stable closed-loop behavior while compensating for the external current.

Due to this control structure, the LNMPC does not converge to the same equilibrium attitude as the PI controller. In the PI case, the heading passively settles to the equilibrium $\gamma_d - \beta$, which arises naturally from the vehicle-current interaction. In contrast, the LNMPC treats the attitude as a controlled variable and regulates it with respect to $\gamma_d - \hat{\beta}$. Consequently, the equilibrium attitude of the LNMPC is not required to coincide with that of the PI controller, and a direct comparison of attitude errors between the two approaches is not strictly equivalent.

This distinction is reflected in the attitude error responses shown in Fig. 6c. The LNMPC exhibits larger transient heading deviations, which

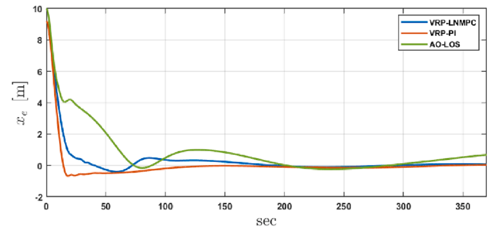

(a) Longitudinal position error x_e.

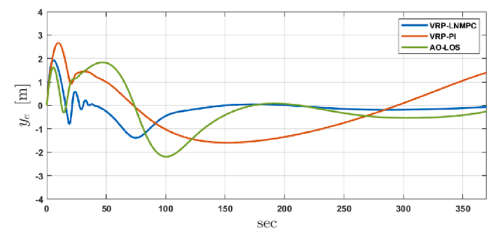

(b) Lateral position error y_e.

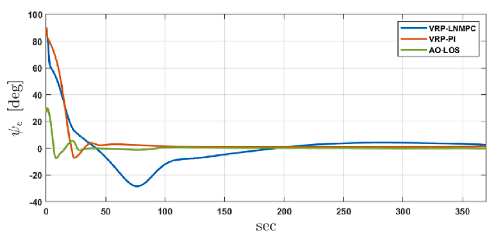

(c) Heading error ψ_e.

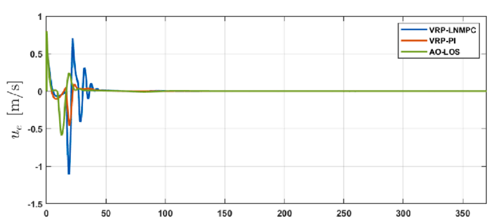

(d) Surge velocity error u_e.

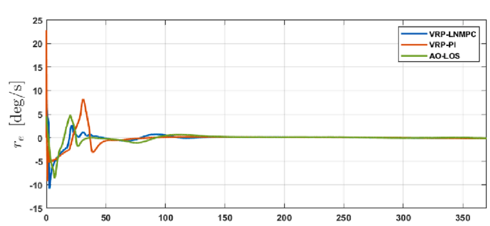

(e) Yaw rate error r_e.

Fig. 6. Tracking performance under constant current conditions. Comparison of position, heading, and velocity errors for the PI, LNMPC, and AO-LOS controllers.

are intentional and result from actively adjusting the attitude to compensate for the current. In contrast, the PI controller converges more directly to its passive equilibrium but lacks the ability to actively adapt the attitude in response to disturbances. Therefore, smaller attitude errors do not necessarily imply superior tracking performance in the constant-current case.

Up to this point, the LNMPC has been compared with the VRP-PI controller. A comparison with the AO-LOS controller is less direct due to the fundamentally different guidance philosophies. The AO-LOS method regulates the vehicle attitude directly to reduce cross-track error, whereas the LNMPC coordinates attitude and position regulation through the vehicle kinematics and dynamics. As a result, while trajectory tracking performance may be comparable, the AO-LOS controller typically achieves more precise attitude regulation.

Another key difference arises from the use of a look-ahead distance in the LOS approach. The cross-track error is corrected at a point ahead of the vehicle rather than at its current position, leading to a smoother but delayed correction. In contrast, the LNMPC corrects errors at the current position while simultaneously regulating attitude, resulting in different transient responses, particularly in the presence of disturbances.

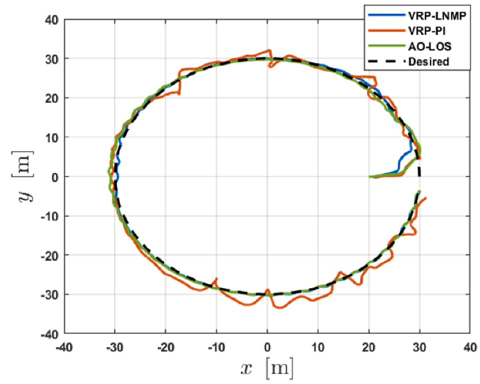

Fig. 7. Vehicle trajectories under time-varying sea current conditions. The comparison illustrates the path-following performance of the PI, LNMPC, and AO-LOS controllers under dynamically changing disturbances.

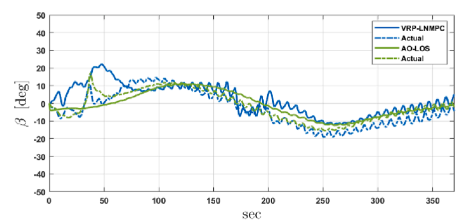

Fig. 8. Estimated sideslip angle $\hat{\beta}$ obtained from the AEKF under time-varying current conditions.

6.1.0.4. (ii) Varying Current:. In this scenario, the vehicle is subjected to a time-varying sea current to evaluate the robustness of the guidance and control strategies under dynamic environmental conditions. The magnitude of the current is kept constant at $V_c = 0.3$ m/s, while the direction varies sinusoidally over time. This scenario represents operating conditions where the vehicle is influenced by changing tidal flows or spatially varying currents, which are common in coastal and shallow-water environments.

The current direction is modeled as a sinusoidal function:

$$\theta_c(t) = A\sin(\omega t) + \theta_{\text{bias}}, \tag{78}$$

where $A = 105°$ is the amplitude, $\theta_{\text{bias}} = -75°$ is the bias, and $\omega = 0.1$ rad/s is the angular frequency.

This time-varying disturbance challenges the controllers to continuously adapt to changing conditions. While the constant-current case allows assessment of nominal tracking performance, the varying current scenario highlights the ability of each controller to reject dynamic disturbances, maintain stability, and minimize tracking errors over time.

Fig. 7 illustrates the vehicle trajectories under a time-varying sea current. In this scenario, the effect of the disturbance is more pronounced, revealing clear differences in the robustness of the considered control strategies.

The PI controller exhibits noticeable oscillations and larger deviations from the reference path. This behavior arises from its passive

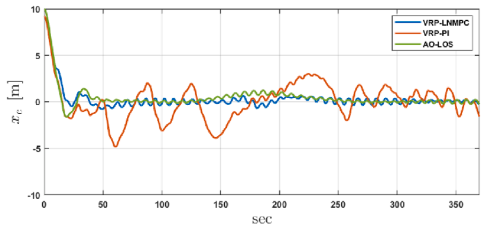

(a) Longitudinal position error x_e.

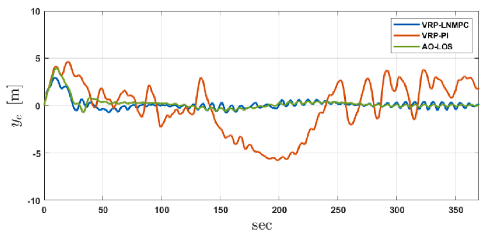

(b) Lateral position error y_e.

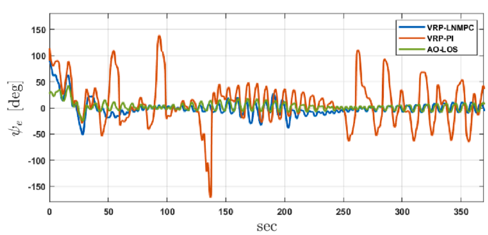

(c) Heading error ψ_e.

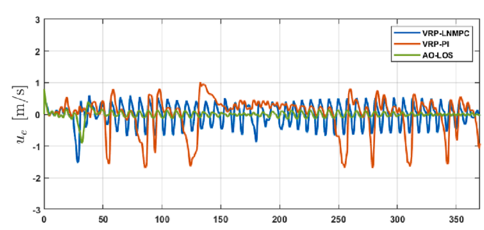

(d) Surge velocity error u_e.

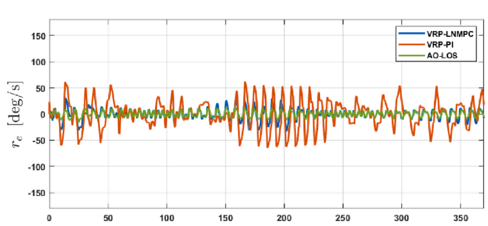

(e) Yaw rate error r_e.

Fig. 9. Tracking performance under time-varying current conditions. Comparison of position, heading, and velocity errors for the PI, LNMPC, and AO-LOS controllers.

attitude response, which is insufficient to counteract rapidly changing current directions. As the external disturbance varies, the lack of explicit attitude regulation causes the vehicle to deviate significantly from the desired trajectory, resulting in degraded tracking performance as shown in Fig. 9.

In contrast, both the AO-LOS and LNMPC controllers demonstrate better robustness under time-varying sea currents, as they explicitly incorporate attitude regulation through β estimation as in Fig. 8. Such disturbance primarily affects the vehicle orientation, hence actively controlling the attitude enables both controllers to better compensate for the varying current and maintain closer adherence to the reference path.

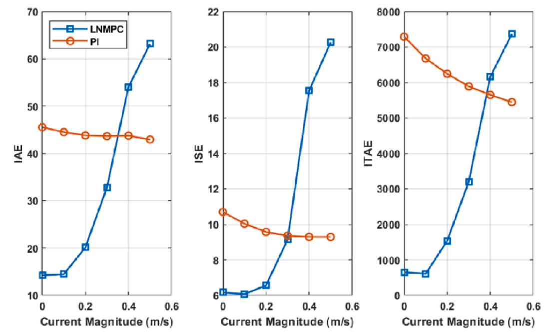

Fig. 10. Robustness analysis under constant current: Tracking performance of the PI and LNMPC controllers.

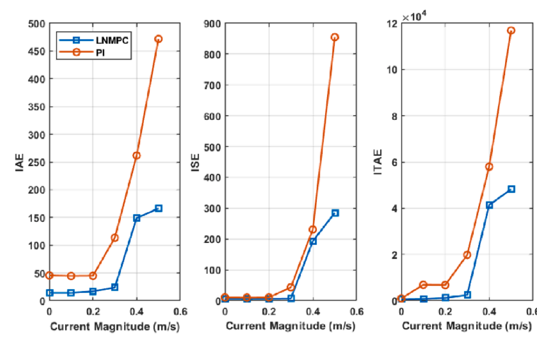

Fig. 11. Robustness analysis under time-varying current: Tracking performance of the PI and LNMPC controllers.

Among the two, the AO-LOS controller achieves slightly better tracking performance. While AO-LOS focuses on minimizing cross-track error through geometric guidance, the VRP-based LNMPC offers greater structural flexibility. In particular, the virtual reference point can be positioned, for instance, at a sensor location thus allowing the controller to track a reference path that does not necessarily coincide with the vehicle's pivoting point. Consequently, the LNMPC should not be viewed as a direct competitor to the LOS approach, but rather as an enhanced alternative framework that offers additional design freedom and robustness under varying operational conditions.

6.2. Robustness analysis

To assess robustness, both controllers are evaluated under constant and time-varying current conditions using the same reference path and initial conditions as in the previous sections. The current magnitude is varied from 0 to 0.5 m/s to examine performance degradation under increasing disturbance intensity.

Tracking performance is quantified using longitudinal, and lateral errors. To ensure fair comparison and avoid scale dominance, all errors are normalized using $x_{e,\max} = 5$ m and $y_{e,\max} = 5$ m. Based on these normalized errors, the Integral of Absolute Error (IAE), Integral of Squared Error (ISE), and Integral of Time-weighted Absolute Error (ITAE) are computed.

The robustness analysis is performed for both constant and time-varying current cases, allowing the influence of disturbance magnitude and temporal variation on controller performance to be systematically evaluated.

In the robustness analysis under constant current conditions, both the PI and LNMPC controllers exhibit stable and bounded tracking performance across the full range of tested current intensities, as shown in Fig. 10. The PI controller displays nearly constant values of the performance indices (IAE, ISE, and ITAE) as the current magnitude increases, indicating strong robustness under steady disturbances. This behavior is expected, as the PI controller converges to a steady equilibrium determined by the balance between vehicle dynamics and the external current.

In contrast, the LNMPC controller achieves lower tracking errors than the PI controller at low current intensities, demonstrating improved accuracy when disturbances are mild. As the current magnitude increases, the performance indices of the LNMPC gradually increase and approach those of the PI controller, as illustrated in Fig. 10. This behavior results from the selected tuning strategy, in which a relatively high weight is assigned to the attitude-related terms in the cost function. Consequently, the controller prioritizes attitude regulation over position correction, which may slightly degrade tracking performance under stronger disturbances. Nevertheless, even in this regime, the overall robustness of the LNMPC remains comparable to that of the PI controller but with additional better attitude regulation.

This behavior highlights an important tuning trade-off inherent to the LNMPC framework. Increasing the attitude weight enhances disturbance rejection–particularly in the presence of varying currents–but may reduce tracking accuracy if excessive control effort is devoted to attitude regulation. Conversely, lowering the attitude weight improves position tracking but weakens robustness to external disturbances. Thus, the tuning parameters provide a mechanism to balance robustness and tracking performance depending on mission requirements.

The benefit of this tuning choice becomes more apparent under time-varying current conditions. As shown in Fig. 11, the PI controller rapidly loses robustness as the disturbance varies, exhibiting increased tracking errors. In contrast, the LNMPC maintains stable and bounded performance, owing to its explicit use of attitude regulation and predictive control structure. While increasing the integral gain of the PI controller could partially improve disturbance rejection, such an approach often leads to oscillatory behavior due to delayed error correction and integral windup.

Overall, these results demonstrate that although both controllers perform comparably under constant disturbances, the LNMPC provides superior robustness to sea current and as a consequence better tracking performance under time-varying conditions. This advantage stems from its ability to exploit attitude regulation and predictive control to accommodate rapidly changing environmental disturbances.

7. Conclusion

This paper presented a VRP-based guidance strategy as an alternative to conventional LOS guidance for a class of AMVs. Unlike traditional VRP approaches that do not explicitly account for attitude dynamics, the proposed framework integrates attitude regulation into the control design, enabling improved robustness against environmental disturbances such as sea currents.

By formulating the tracking error dynamics in the body-fixed frame, both cross-track and heading errors are addressed simultaneously through yaw-rate control. Based on this formulation, an LNMPC was developed to jointly regulate position and attitude. An AEKF was employed to estimate the sideslip angle β, allowing for a consistent attitude representation in the presence of unknown and time-varying sea currents.

Simulation results demonstrate that incorporating the estimated sideslip into the prediction model enhances disturbance rejection, particularly under time-varying current conditions. Compared to the VRP-PI controller, the proposed LNMPC exhibits improved robustness and stability, while achieving comparable or improved position-tracking performance in constant-current scenarios. The benefits of explicit attitude regulation become more pronounced as environmental disturbances increase, where PI kinematic control strategies tend to degrade.

At the same time, the proposed approach introduces additional computational complexity due to the online optimization required by the LNMPC, which may limit applicability in systems with strict real-time constraints. Moreover, although attitude regulation improves robustness, it does not necessarily guarantee superior attitude tracking compared to LOS-based methods, owing to fundamental differences in control objectives and structure.

Nevertheless, the proposed framework offers increased flexibility through the use of a virtual reference point, which can be positioned independently of the vehicle's center of mass. This allows the controller to better accommodate sensor placement, vehicle geometry, and task-specific requirements, making it a complementary alternative rather than a replacement for LOS-based guidance.

Future work will focus on experimental validation of the controller on a physical marine vehicle and extending the framework to accommodate more advanced scenarios, such as obstacle avoidance and time-varying path planning. Additionally, the proposed methodology can be adapted to vehicles with vertical control (e.g., using pitch to regulate depth), where attitude control becomes even more critical. As discussed in Degorre et al. (2024a), VRP-based guidance has the potential to address underactuation via kinematic coupling, but it may lead to undesirable attitude configurations (e.g., inverted tracking). The proposed approach offers a robust solution to such issues and enables VRP guidance to be effectively applied to reconfigurable and more complex marine vehicles.

CRediT authorship contribution statement

S. K. Mallipeddi: Writing – review & editing, Writing – original draft, Validation, Methodology, Investigation, Formal analysis, Conceptualization; **M. Menghini:** Writing – review & editing, Investigation, Conceptualization; **S. Simani:** Writing – review & editing, Supervision, Conceptualization; **P. Castaldi:** Writing – review & editing, Writing – original draft, Supervision, Investigation, Conceptualization.

Data availability

Data will be made available on request.

Declaration of competing interest

The authors declare that they have no known competing financial interests or personal relationships that could have appeared to influence the work reported in this paper.

The author is an Editorial Board Member/Editor-in-Chief/Associate Editor/Guest Editor for [Journal name] and was not involved in the editorial review or the decision to publish this article.

During the preparation of this work, the author(s) used ChatGPT by OpenAI to assist with language editing, improving clarity, and refining the structure of technical content. After using this tool, the author(s) reviewed and edited the content as necessary and take(s) full responsibility for the final version of the manuscript.

Supplementary material

Supplementary material associated with this article can be found in the online version at 10.1016/j.conengprac.2026.106769.

References

Alonge, F., D'Ippolito, F., & Raimondi, F. M. (2001). Trajectory tracking of underactuated underwater vehicles. In *Proceedings of the 40th IEEE conference on decision and control (cat. no. 01CH37228)* (pp. 4421–4426). IEEE (*vol. 5*).

Belleter, D., Maghenem, M. A., Paliotta, C., & Pettersen, K. Y. (2019). Observer based path following for underactuated marine vessels in the presence of ocean currents: A global approach. *Automatica*, *100*, 123–134.

Berge, S. P., Ohtsu, K., & Fossen, T. I. (1998). Nonlinear control of ships minimizing the position tracking errors. *IFAC Proceedings Volumes*, *31*(30), 129–134.

Besançon, G., Bornard, G., & Hammouri, H. (1996). Observer synthesis for a class of nonlinear control systems. *European Journal of control*, *2*(3), 176–192.

Besancon, G., de León-Morales, J., & Huerta-Guevara, O. (2006). On adaptive observers for state affine systems. *International Journal of Control*, *79*(06), 581–591.

Bhat, S., & Stenius, I. (2018). Hydrobatics: A review of trends, challenges and opportunities for efficient and agile underactuated auvs. In *2018 IEEE/OES Autonomous underwater vehicle workshop (AUV)* (pp. 1–8). IEEE.

Boretti, A. (2024). Unmanned surface vehicles for naval warfare and maritime security. *The Journal of Defense Modeling and Simulation*, (p. 15485129241283056).

Breivik, M., & Fossen, T. I. (2005). Principles of guidance-based path following in 2D and 3D. In *Proceedings of the 44th IEEE conference on decision and control* (pp. 627–634). IEEE.

Caharija, W., Pettersen, K. Y., Bibuli, M., Calado, P., Zereik, E., Braga, J., Gravdahl, J. T., Sørensen, A. J., Milovanović, M., & Bruzzone, G. (2016). Integral line-of-sight guidance and control of underactuated marine vehicles: Theory, simulations, and experiments. *IEEE Transactions on Control Systems Technology*, *24*(5), 1623–1642.

Caharija, W., Pettersen, K. Y., Calado, P., & Braga, J. (2015). A comparison between the ILOS guidance and the vector field guidance. *IFAC-PapersOnLine*, *48*(16), 89–94.

Degorre, L., Fossen, T. I., Chocron, O., & Delaleau, E. (2024a). A model-based kinematic guidance method for control of underactuated autonomous underwater vehicles. *Control Engineering Practice*, *152*, 106068.

Degorre, L., Fossen, T. I., Delaleau, E., & Chocron, O. (2024b). A virtual reference point kinematic guidance law for 3-d path-following of autonomous underwater vehicles. *IEEE Access 12*, 109822–109831. https://doi.org/10.1109/ACCESS.2024.3440659

Degorre, L., Lapierre, L., & Belier, T. (2025). New formulation and experimental validation of the kinematic guidance principle on an underactuated uncrewed surface vessel. In *IFAC mechatronics and robotics symposia*.

Di Ciaccio, F., & Troisi, S. (2021). Monitoring marine environments with autonomous underwater vehicles: A bibliometric analysis. *Results in Engineering*, *9*, 100205.

Do, K. D., & Pan, J. (2009). Control of ships and underwater vehicles: Design for underactuated and nonlinear marine systems. Springer Science & Business Media.

Fossen, T. I. (2011). Handbook of marine craft hydrodynamics and motion control. John Wiley & Sons.

Fossen, T. I. (2023). An adaptive line-of-sight (ALOS) guidance law for path following of aircraft and marine craft. *IEEE Transactions on Control Systems Technology*, *31*(6), 2887–2894.

Fossen, T. I., & Aguiar, A. P. (2024). A uniform semiglobal exponential stable adaptive line-of-sight (ALOS) guidance law for 3-D path following. *Automatica*, *163*, 111556.

Fossen, T. I., Breivik, M., & Skjetne, R. (2003). Line-of-sight path following of underactuated marine craft. *IFAC Proceedings Volumes*, *36*(21), 211–216.

Fossen, T. I., & Pettersen, K. Y (2014). On uniform semiglobal exponential stability (USGES) of proportional line-of-sight guidance laws. *Automatica*, *50*(11), 2912–2917.

Fossen, T. I., Pettersen, K. Y., & Galeazzi, R. (2014). Line-of-sight path following for dubins paths with adaptive sideslip compensation of drift forces. *IEEE Transactions on Control Systems Technology*, *23*(2), 820–827.

Grandia, R., Taylor, A. J., Singletary, A., Hutter, M., & Ames, A. D. (2020). Nonlinear model predictive control of robotic systems with control lyapunov functions. arXiv preprint arXiv:2006.01229

Gu, N., Wang, D., Peng, Z., Wang, J., & Han, Q.-L. (2022). Advances in line-of-sight guidance for path following of autonomous marine vehicles: An overview. *IEEE Transactions on Systems, Man, and Cybernetics: Systems*, *53*(1), 12–28.

Khalil, H. K., & Grizzle, J. W. (2002). Nonlinear systems (vol. 3). Prentice Hall Upper Saddle River, NJ.

Kim, B. S., Calise, A. J., & Sattigeri, R. J. (2007). Adaptive, integrated guidance and control design for line-of-sight-based formation flight. *Journal of Guidance, Control, and Dynamics*, *30*(5), 1386–1399.

Lapierre, L., & Soetanto, D. (2007). Nonlinear path-following control of an AUV. *Ocean Engineering*, *34*(11-12), 1734–1744.

Lekkas, A. M., & Fossen, T. I. (2012). A time-varying lookahead distance guidance law for path following. *IFAC Proceedings Volumes*, *45*(27), 398–403.

Liu, L., Wang, D., & Peng, Z. (2016). ESO-based line-of-sight guidance law for path following of underactuated marine surface vehicles with exact sideslip compensation. *IEEE Journal of Oceanic Engineering*, *42*(2), 477–487.

Mansor, H., Norhisam, M. H., Abidin, Z. Z., & Gunawan, T. S. (2021). Autonomous surface vessel for search and rescue operation. *Bulletin of Electrical Engineering and Informatics*, *10*(3), 1701–1708.

Martinović, L., Zečević, Ž., Bibuli, M., Caccia, M., & Nađ, Đ. (2024). Adaptive observer-based line-of-sight guidance law for path following of underactuated unmanned surface vehicle with sideslip compensation. *IEEE Access*, *12*, 144992–145002. https://doi.org/10.1109/ACCESS.2024.3471790

Matouš, J., Paliotta, C., Pettersen, K. Y., & Varagnolo, D. (2024). The hand position concept for control of underactuated underwater vehicles. *IEEE Transactions on Control Systems Technology*, *32*(6), 2223–2239. https://doi.org/10.1109/TCST.2024.3412529

Matouš, J., Pettersen, K. Y., Varagnolo, D., Paliotta, C., & Ruud, E.-L. (2025). Adaptive hand position for underactuated underwater vehicles. *IEEE Journal of Oceanic Engineering*, *50*(3), 1647–1656. https://doi.org/10.1109/JOE.2024.3511708

Menghini, M., Mallipeddi, S. K., Castaldi, P., & De Marchi, L. (2024a). Neuro adaptive integral sliding mode control based on composite learning for path following of underactuated underwater vehicle: Blucy. In *Conference proceedings of iSCSS*. (*vol. 2024*).

Menghini, M., Mallipeddi, S. K., De Marchi, L., & Castaldi, P. (2024b). Modelling and parameter identification of UUV blucy for control design: A benchmark model. *Ocean Engineering*, *313*, 119617.

Nauert, F., & Kampmann, P. (2023). Inspection and maintenance of industrial infrastructure with autonomous underwater robots. *Frontiers in Robotics and AI*, *10*, 1240276.

Nie, J., & Lin, X. (2019). Improved adaptive integral line-of-sight guidance law and adaptive fuzzy path following control for underactuated MSV. *ISA Transactions*, *94*, 151–163.

Paliotta, C., Lefeber, E., Pettersen, K. Y., Pinto, J., Costa, M. et al. (2018). Trajectory tracking and path following for underactuated marine vehicles. *IEEE Transactions on Control Systems Technology*, *27*(4), 1423–1437.

Pavlov, A., Nordahl, H., & Breivik, M. (2009). MPC-based optimal path following for underactuated vessels. *IFAC Proceedings Volumes*, *42*(18), 340–345.

Pettersen, K. Y., & Egeland, O. (2002). Time-varying exponential stabilization of the position and attitude of an underactuated autonomous underwater vehicle. *IEEE Transactions on Automatic Control*, *44*(1), 112–115.

Pettersen, K. Y., & Nijmeijer, H. (2001). Underactuated ship tracking control: Theory and experiments. *International Journal of Control*, *74*(14), 1435–1446.

Whitt, C., Pearlman, J., Polagye, B., Caimi, F., Muller-Karger, F., Copping, A., Spence, H., Madhusudhana, S., Kirkwood, W., Grosjean, L. et al. (2020). Future vision for autonomous ocean observations. *Frontiers in Marine Science*, *7*, 697.

Xu, H., Fossen, T. I., & Soares, C. G. (2020). Uniformly semiglobally exponential stability of vector field guidance law and autopilot for path-following. *European Journal of Control*, *53*, 88–97.

Zhang, Y., Li, S., Wang, W., Wang, S., & Mu, R. (2024). Three-dimensional path following control of underactuated autonomous underwater vehicles with nonzero roll dynamics: A novel line-of-sight-guided approach. *International Journal of Robust and Nonlinear Control*, *34*(8), 4959–4977.